Examining the Effect of Varying Bragg Grating and Fabry-Perot Cavity Parameters on the Optical Transmission of a Semiconductor Laser

Travis Innes - 28564383
Department of Electrical and Computer Engineering
University of British Columbia, Vancouver, BC, V6T1Z4, Canada

***Abstract*—This research paper investigates the influence of parameter variations in a Fabry-Perot Cavity and Bragg Gratings on optical transmission. By hypothesizing, simulating, and fabricating 11 different photonic integrated circuits which resonate at 1310nm we will explore the impact of two main parameters: I. The effect of varying length of the Fabry-Perot Cavity and II. The effect of varying the Bragg-Grating period.**

I. Introduction

In an era with increasing reliance on digital connectivity and data-driven applications, the demand for faster, more reliable, and energy-efficient communication technologies have become paramount. The application of optical waveguides, photonic circuits, and semiconducting lasers have become increasingly viable mediums for the next generation of compute, promising high bandwidth, low loss, and lightning speed.

This paper will explore some of the basic ways to apply these applications such as the use of Bragg-Gratings and Fabry-Perot Cavities within a semiconductor to control the transmission spectra, how to model these types of systems, and how changing a chosen set of parameters impact transmission. Specifically, exploring how the change of number of periods in a Bragg-Grating and length of a Fabry-Perot cavity will influence the transmission and quality factor of a laser at a wavelength centered at 1310nm.

Fabrication of our test vehicles will be done by Applied Nanotools (ANT) on an oxide cladded chip and printed on a single mask layer. Measurement of the test vehicles and data collection will be done by the University of British Columbia.

II. Theory And Model Description

A. Bragg Gratings

In the field of semi-conductor lasers, Bragg-Gratings (Figure 1) are used as a type of optical filter which reflect a select spectrum of wavelength. The region of reflected wavelength is called the Bragg wavelength (Figure 2) and defined as:

$$\lambda_B = 2n_{eff}\Lambda$$

Where n_{eff} is the effective index of refraction and lamda (Λ) is the period of the Bragg grating. By etching small notches into a SiO_2 waveguide fiber an alternating index of refraction at a period (Λ) is effectively created. This allows the creation of an alternating index of refraction without the need for alternating materials and acts as a filter to reflect a chosen wavelength and transmit all other wavelengths. In electronics this type of filter is commonly called a bandstop filter.

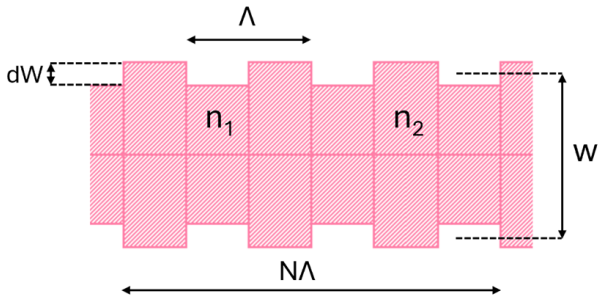

Fig. 1: Bragg Grating

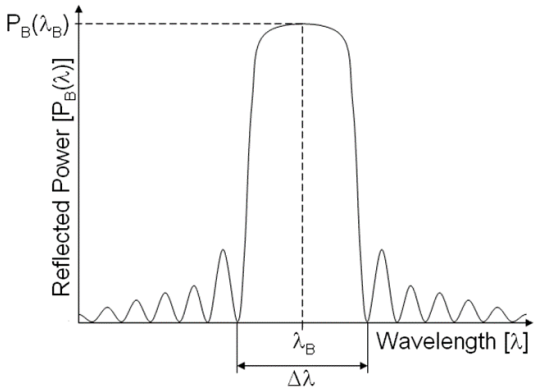

Fig. 2: Reflection spectrum example of a Bragg grating to illustrate the Bragg wavelength (λ_B). Image from "Fiber Bragg Grating," Wikipedia, Dec. 15, 2019.

B. Fabry-Perot Cavity

In the opposing realm, the Fabry-Perot Cavity acts as an optical filter that acts to transmit a chosen wavelength and reflect all other wavelengths (Figure 3). The cavity consists of two sets of parallel mirrors with length (L) between them and only transmits wavelengths that are in resonance with the cavity. The range of transmission is dependent on the

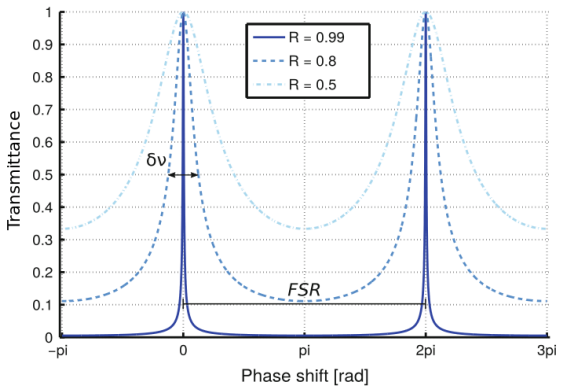

Fig. 3: Transmission spectrum of a Fabry-Perot cavity. Image from Mejia Morales, Julian. (2021), Acoustofluidic interferometric device for optomechanical cytometry.

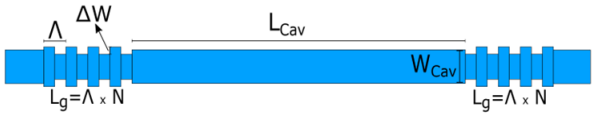

Fig. 4: Two Bragg gratings and a Fabry Perot Cavity. Image from Ajay Mistry (2023) "Design of a Fabry-Perot cavity based on phase-shifted Bragg gratings"

reflectivity (R) of the mirrors (Figure 3) and determines the quality Q of the cavity. Higher reflectivity of the mirrors results in more internal cavity reflections, which causes a narrower transmission range, thus increased intensity, and in turn allows the highest efficiency gain of the laser. The number of peaks is a function of the length:

$$V_{FSR} = \frac{c}{2L}$$

The combination of both the Bragg-Grating and Fabry-Perot cavity allows for a very narrow region of transmission as seen in Figure 4.

III. Simulation Results

A. Simulating the Waveguide - MODE

Adhering to fabrication requirements, a geometry of 220nm x 350nm is chosen to create a single mode optical waveguide using Lumerical MODE. Here, the silicon oxide (SiO2) waveguide lays atop a silicon oxide SiO2 cladding while exposed to open air. MODE allows accurate analysis of the TE response along the waveguide based on our dimensions and materials as seen in Figure 5.

Through MODE a frequency sweep at wavelengths $1300nm < \lambda < 1400nm$ can be taken to compare the impact wavelength has on the effective index (n_{eff}) as seen in Figure 6.

From these simulations a group index of 4.51 ($n_g = 4.51$) and effective index of 2.44 ($n_{eff} = 2.44$) is found. Extracting from MODE, the grating waveguide compact model Taylor

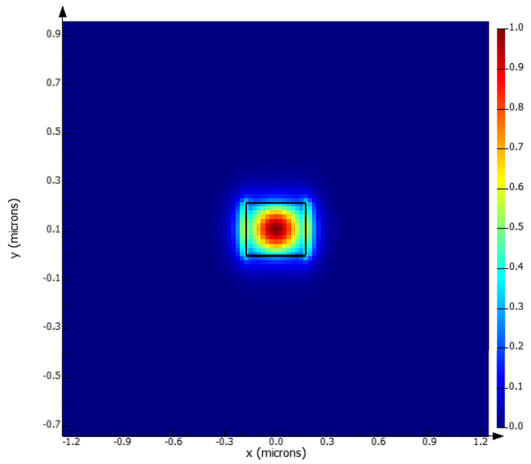

Fig. 5: Simulated Lumerical MODE response from cross section of waveguide at geometry 220nm x 350 with λ_B = 1310nm

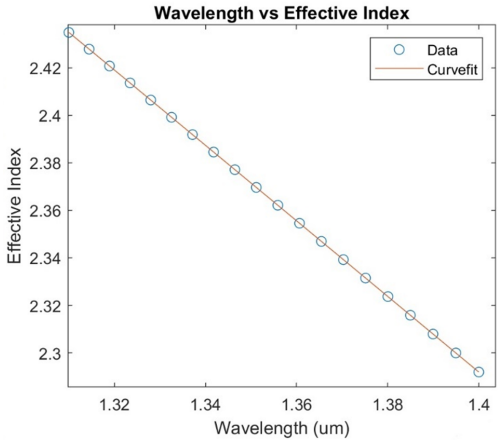

Fig. 6: Wavelength vs Effective index via Lumerical MODE frequency sweep, curvefit in brown using third order Taylor expansion approximation

expansion from the simulated parameters given $n_0 = 4.33$, $n_1 = -1.32$, $n_2 = -0.091$:

$$n_{eff}(\lambda) = 4.33 + 1.32(\lambda - \lambda_0) + 0.091(\lambda - \lambda_0)^2$$

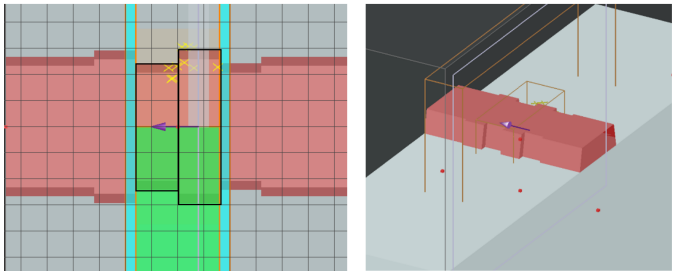

Fig. 7: Lumerical FDTD single period of Bragg Grating top view (left) and isometric view (right)

B. Simulating a Bragg-Grating Period - FDTD

A single period with length 272nm of Bragg-Grating is simulated using FDTD (Figure 7), short for Finite-Difference Time-Domain, a program which solves Maxwell's equations for nano-scale optical designs. A corrugation width (dW) of 50nm is used, device rib of 90nm, substate thickness 2um, and sidewall angle of 90 degrees. This simulation brings together the period length (Λ) and delta Lambda ($\Delta\Lambda$) at the Bragg wavelength (1310nm). The grating coupler coefficient (κ) can be solved for:

$$\kappa = \pi n_g \frac{\Delta\lambda}{\lambda_B^2}$$

This parameter is essential for the implementation of an accurate Bragg-grating design and will be used to model our transmission spectra in Interconnect. Applying the formula to our simulated values a grating coupler coefficient (κ) of 149,706 can be found.

C. Matlab Simulation - TMM

TMM, or the Transfer-Matrix Method, is a method of matrix analysis that is used to describe the result of propagating waves through changing mediums. Using the TMM simplifies calculating the response of a grating coupler design. The transfer matrix method for a homogeneous section of waveguide is defined by Dr. Lukas Chrostowski and Dr. Michael Hochberg in Silicon Photonics Design: From Devices to Systems as such:

$$T_{hw} = \begin{bmatrix} e^{j\beta L} & 0 \\ 0 & e^{-j\beta L} \end{bmatrix}$$

Where $\beta = 2\pi\frac{n_{eff}}{\lambda} - i\frac{\alpha}{2}$, α being loss of -3dB/cm. The region separating the two different homogeneous materials can be defined using the matrix:

$$T_{is-12} = \begin{bmatrix} 1/t & r/t \\ r/t & 1/t \end{bmatrix} = \begin{bmatrix} \frac{n_1+n_2}{2\sqrt{n_1 n_2}} & \frac{n_1-n_2}{2\sqrt{n_1 n_2}} \\ \frac{n_1-n_2}{2\sqrt{n_1 n_2}} & \frac{n_1+n_2}{2\sqrt{n_1 n_2}} \end{bmatrix}$$

Separating the response of the material and response of the barrier between material a model can be created for a Bragg Grating:

$$T = (T_{hw-2}T_{hw-21}T_{hw-1}T_{hw-12})^N$$

$$T = [(T_p)^N)]T_{hw-2}[(T_p)^N)]T_{hw-2}$$

Using these transfer matrix definitions, reflection/transmission models can be cascaded together to represent Bragg gratings and a Fabry Perot cavity. This allows the easy creation of transmission/reflection responses given the index of refraction of our materials (n_1/n_2), β, period length (Λ), period number (N), and wavelength (λ). Using the values generated from MODE and FDTD, a Bragg grating with period 110, cavity length 87um, and using TMM to visualize the transmission/reflection, we get Figure 8.

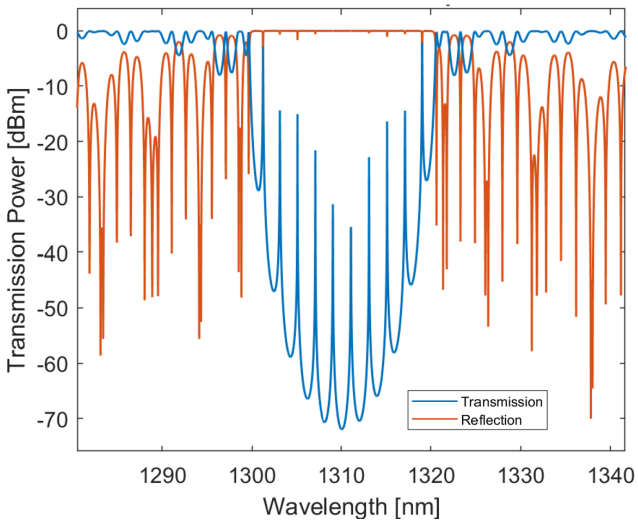

Fig. 8: TMM transmission/reflection spectra taken using FDTD/MODE parameters, 87um Fabry-Perot and 110 Bragg periods

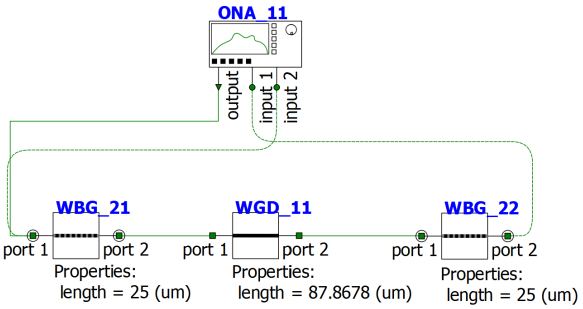

Fig. 9: Lumerical INTERCONNECT circuit diagram showing Fabry-Perot cavity encased by two Bragg gratings

D. Simulating the Full Circuit - INTERCONNECT

Understanding the practical use of the parameters through tuning the TMM model, a more comprehensive simulation of a full photonic circuit can be put together using Lumerical Interconnect (Figure 9).

From these simulations we generate a preliminary quality factor of approximately 90,000. Interconnect will be used in the following steps as the final simulation before layout (Figure 10).

E. Design Methodology

Two main parameters will be varied throughout the design: (1) the number of Bragg-Grating periods in each photonic circuit and (2) the length of the cavity. The optimization will be based on the quality factor of the device which is defined as:

$$Q = \frac{\lambda_0}{\Delta\lambda_{3dB}}$$

Where λ_0 is the wavelength at which transmission occurs in the Fabry-Perot cavity, and $\Delta\lambda_{3dB}$ is the 3dB bandwidth

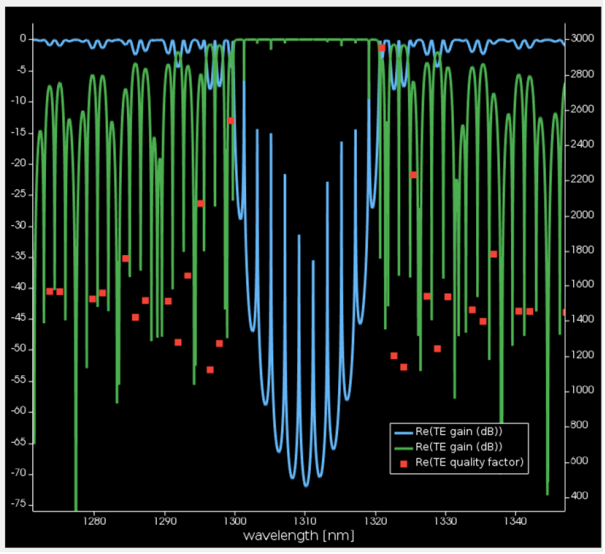

Fig. 10: Simulated transmission spectra from Lumerical INTERCONNECT

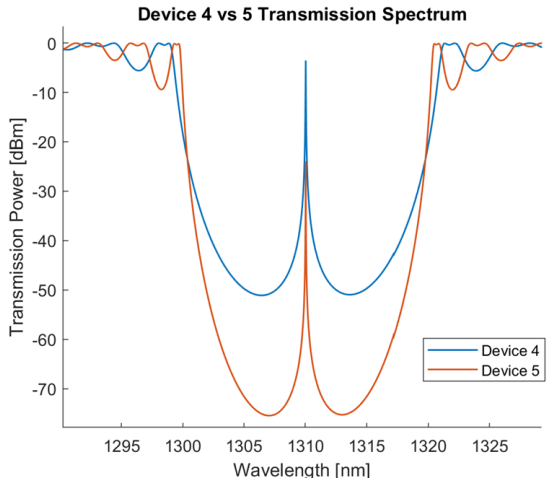

Fig. 11: 25um (Device 4) vs 35um (Device 5) Bragg grating transmission

width of the transmission peak. The goal is to see how each parameter influences the movement of the quality factor (Q) as well as which external observed factors to take into account when considering the highest quality factor (Q).

The Bragg-Gratings are optical filters which reflect the transmitted signal. Longer Bragg-Gratings cause transmission peaks, thus quality factor (Q), to be sharper, but overall losses to be higher. Figure 11 illustrates the difference in transmission between 25um (Device 4) and 35um (Device 5) Bragg-Gratings.

The Fabry-Perot cavity only transmits wavelengths that are in resonance with the cavity, thus creating a larger cavity at intervals of the resonance frequency creates additional modes that can be transmitted. Figure 12 illustrates the difference in transmission between a short and long cavity, 4.4um (Device 4) vs 87um (Device 8).

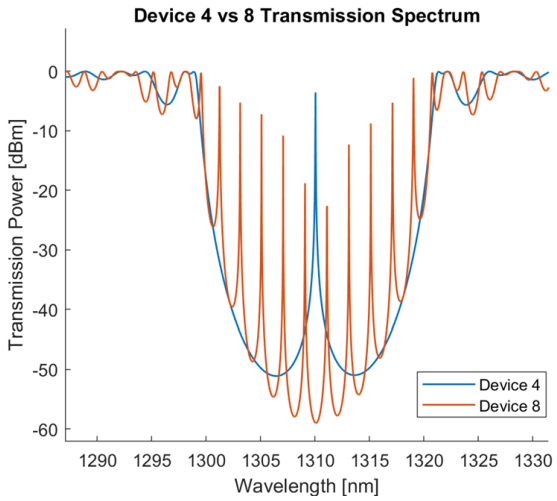

Fig. 12: 4.4um (Device 4) vs 87um (Device 8) Fabry-Perot transmission

For this paper 11 designs were created: 9 optical circuits and 2 look back circuits to analyze the loss experienced though the grating couplers and waveguides. The designs are numbered in Table 1 with varying values of Bragg grating period number and cavity length.

TABLE I: Test Devices and Their Characteristics

	Cavity Length (um)	*Bragg Grating Periods*	*Q Factor*
Device 1	4.4	110	81875
Device 2	8.8	110	52400
Device 3	17.5	110	65500
Device 4	4.4	92	77058
Device 5	4.4	129	131000
Device 6	40.5	92	137894
Device 7	87	92	218333
Device 8	87	110	87333
Device 9	87	129	109166

F. Simulation Results

Simulation results of the transmission of devices 1,3,6,8 are shown in Figure 13.

IV. Mask Layout

KLayout is used to implement the mask (Figure 14). SiEPIC Tools is used to add integrated optics / silicon photonics functionality (waveguides, netlist extraction, circuit simulations, etc) to the proposed designs. In total 11 designs are included, 9 to test parameter changes and 2 reference lookback structures to measure optical loss against.

V. Fabrication

The photonic devices were fabricated using the NanoSOI MPW fabrication process by Applied Nanotools Inc. (http://www.appliednt.com/nanosoi; Edmonton, Canada) which is based on direct-write 100 keV electron beam lithography technology. Silicon-on-insulator wafers of 200 mm diameter, 220 nm device thickness and 2 µm buffer oxide

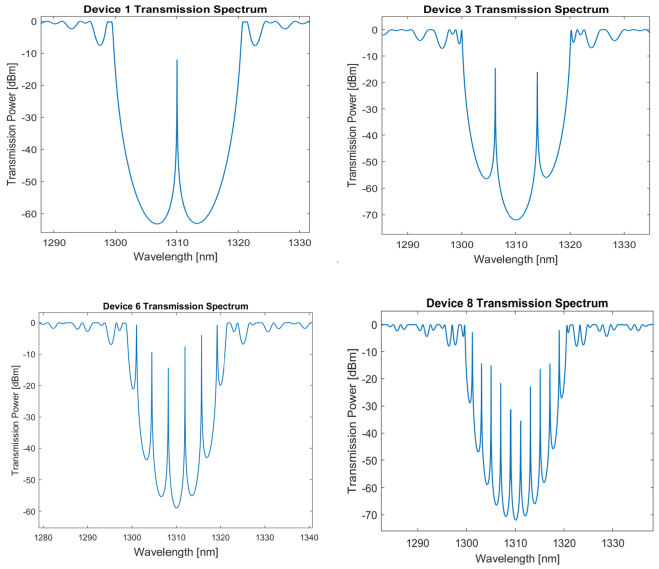

Fig. 13: Device 1, 3, 6, 8 transmission

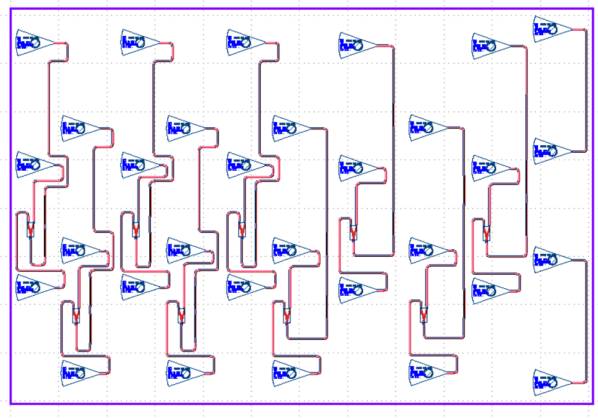

Fig. 14: KLayout layout of photonic circuits

thickness are used as the base material for the fabrication. The wafer was pre-diced into square substrates with dimensions of 25x25 mm, and lines were scribed into the substrate backsides to facilitate easy separation into smaller chips once fabrication was complete. After an initial wafer clean using piranha solution (3:1 H2SO4:H2O2) for 15 minutes and water/IPA rinse, hydrogen silsesquioxane (HSQ) resist was spin-coated onto the substrate and heated to evaporate the solvent. The photonic devices were patterned using a Raith EBPG 5000+ electron beam instrument using a raster step size of 5 nm. The exposure dosage of the design was corrected for proximity effects that result from the backscatter of electrons from exposure of nearby features. Shape writing order was optimized for efficient patterning and minimal beam drift. After the e-beam exposure and subsequent development with a tetramethylammonium sulfate (TMAH) solution, the devices were inspected optically for residues and/or defects. The chips were then mounted on a 4" handle wafer and underwent an anisotropic ICP-RIE etch process

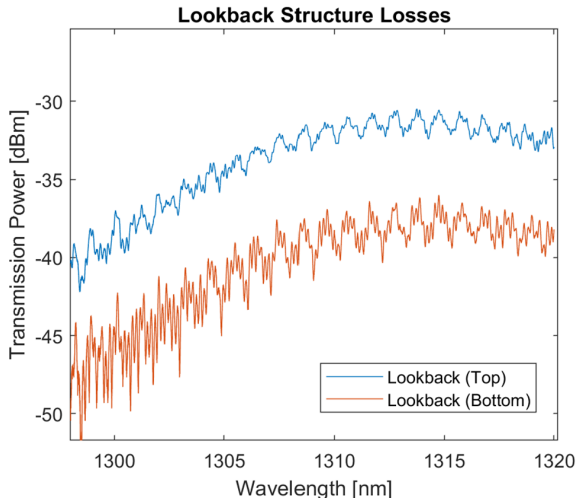

Fig. 15: Losses from lookback structures (Device 10/11)

using chlorine after qualification of the etch rate. The resist was removed from the surface of the devices using a 10:1 buffer oxide wet etch, and the devices were inspected using a scanning electron microscope (SEM) to verify patterning and etch quality. A 2.2 µm oxide cladding was deposited using a plasma-enhanced chemical vapour deposition (PECVD) process based on tetraethyl orthosilicate (TEOS) at 300ºC. Reflectrometry measurements were performed throughout the process to verify the device layer, buffer oxide and cladding thicknesses before delivery.

VI. Measurement

To characterize the devices, a custom-built automated test setup [2, 6] with automated control software written in Python was used [3]. An Agilent 81600B tunable laser was used as the input source and Agilent 81635A optical power sensors as the output detectors. The wavelength was swept from 1500 to 1600 nm in 10 pm steps (or 1 pm steps for those that requested it). A polarization maintaining (PM) fibre was used to maintain the polarization state of the light, to couple the TE polarization into the grating couplers [4] (or TM if you designed your circuits for TM, in which case a 90º rotation was used to inject light into the TM grating couplers [4]). A polarization maintaining fibre array was used to couple light in/out of the chip [5].

VII. Experimental Data

Device 10 and 11 quantify the dB loss (Figure 15) from the grating couplers and waveguides. The average for a majority of the losses in the lookback structures in the range of interest $1300 < \lambda < 1320$ is approximately -35dB. We will add this to the y-axis of our experimental data to compare our results on a similar scale (Figure 16).

From our submitted experiments only two resulted in usable data: device 8 and device 6. Both devices used long cavities and transmitted peaks at the edges of their transmission spectrum. There are a few possible explanations for this: (1)

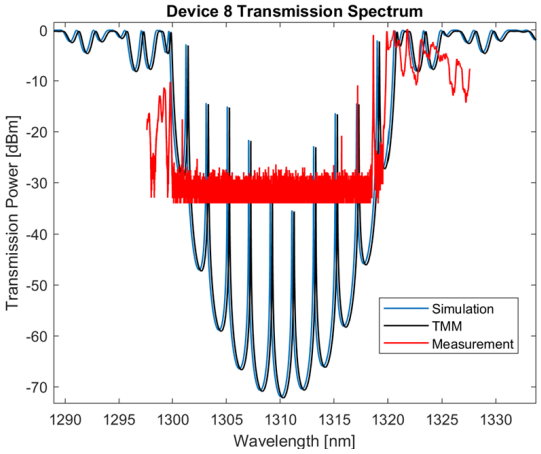

Fig. 16: Device 8 transmission: calculation vs simulation vs measurement

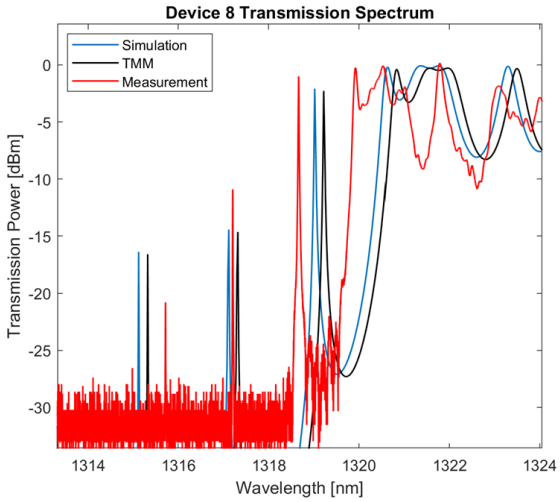

Fig. 17: Device 8 examined for observable peaks

The losses from the grating couplers proved to be higher than predicted and Optical Spectrum Analyzer (OSA) noise floor was above our transmitted data or (2) our quality factor was so high that it proved to be above the sampling frequency. However, the transmission peaks from the observable data from device 6 and device 8 show that even with a simulated loss of approximately -20dB there is still visible transmission. Device 1 and device 3 had similar loss in their transmission spectrum, however, their peaks were simulated to be transmitted in the middle of the transmission's spectrum. This suggest that it was not the level of loss that was the determining factor, but the sampling frequency. This hypothesis is strengthened by the observation of how much higher the quality factor (Q) is within the center of the transmission spectrum in our simulated designs. A high quality factor (Q) is categorized by a small 3dB bandwidth region, meaning the higher the quality factor the lower the sampling resolution of the transmission peak.

Thus, observing the results of the sampling it can be reasoned that the sampling frequency wasn't high enough to record the higher quality factor (Q) transmission peaks.

Figure 16 illustrates the result of the Lumerical Interconnect Simulation, Transfer Matrix Method (TMM) Simulation, and our device data aligned. The simulations show to be predictive of our data at the fringes of the design as seen in Figure 17.

VIII. Analysis

Zooming into the peaks on the fringes of device 8, a Lorentzian curve fit (Figure 18) can be made to estimate the data points and calculate an accurate quality factor (Q) by estimating the 3dB coordinates. A quality factor (Q) of 146k is found from our fringe peaks in device 8.

IX. Discussion

Overall, the quality factor from the simulated models was very similar to that of the experimental data. Out of the two designs that showed significant data, our highest quality factor recorded was 146k. For device 8 this was lower than the predicted 218k.

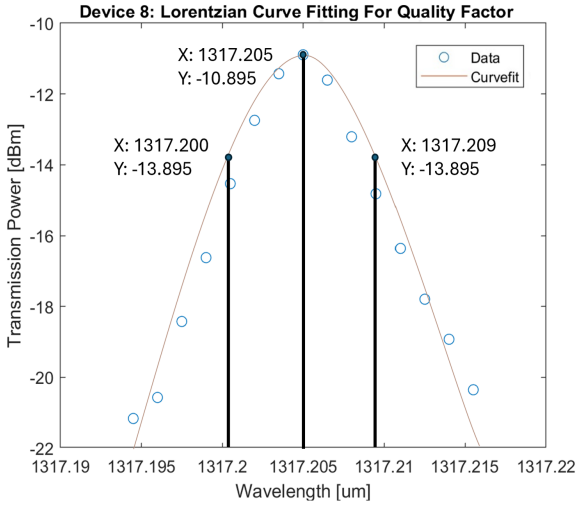

Fig. 18: Device 8 peak fit with a Lorentzian curve for precise quality factor measurement

X. Conclusion

This paper has explored the influence of parameter variations in a Fabry-Perot Cavity and Bragg Gratings on optical transmission. Exploring the impact of two main parameters: I. The effect of varying length of a Fabry-Perot Cavity which resonates at 1310nm and II. The effect of varying the Bragg-Grating period and it's implications on the quality factor (Q) of a design.

Given only two of the nine devices that we created resulted in usable data, the measuring equipment played a larger roll in observable quality factor than expected. In future experiments, it will be noted that understanding the specifications of the measuring equipment is extremely important to finding conclusive data.

Overall, increased Bragg-Gratings size were shown to have a minor increased result in quality factor but at the expense of a larger loss. While, based on the data, the size of the

Fabry-Perot cavity seems to have no apparent impact on the quality factor, however, due to the increase in transmission peaks, allows is to have many more peaks to draw samples from.

XI. Acknowledgments

I acknowledge the edX UBCx Phot1x Silicon Photonics Design, Fabrication and Data Analysis course, which is supported by the Natural Sciences and Engineering Research Council of Canada (NSERC) Silicon Electronic-Photonic Integrated Circuits (SiEPIC) Program. The devices were fabricated by Applied Nanotools, Inc. Iman Taghavi performed the measurements at The University of British Columbia. We acknowledge Lumerical Solutions, Inc., Mathworks, Python, and KLayout for the design software.

References

[1] L. Chrostowski and M. Hochberg, Silicon Photonics Design. Cambridge University Press, 2015.
[2] L. Chrostowski, "ELEC 413 Project 1 2– Fabrication process details" SiEPIC FAB, Vancouver, 2023.
[3] L. Chrostowski, "Bragg Reflectors, VCSELs, Transfer Matrix Method, Waveguide Bragg Gratings, Bragg cavity design", 2021.
[4] Wikipedia Contributors, "Fiber Bragg grating," Wikipedia, Dec. 15, 2019. $https://en.wikipedia.org/wiki/Fiber_bragg_grating$
[5] L. Chrostowski, "ELEC 413 Semiconductor Lasers Waveguide Fabry Perot Cavities" SiEPIC FAB, 2023.
[6] H. Zou, "A Study of the Effect of Varying Bragg Grating Parameters on a Fabry-Perot Cavity Design," 2023.
[7] B. Lin, Design and Evaluation of Bragg Grating Cavity Devices with High Quality Factor, 2023.
[8] http://siepic.ubc.ca/probestation, using Python code developed by Michael Caverley.
[9] Yun Wang, Xu Wang, Jonas Flueckiger, Han Yun, Wei Shi, Richard Bojko, Nicolas A. F. Jaeger, Lukas Chrostowski, "Focusing sub-wavelength grating couplers with low back reflections for rapid prototyping of silicon photonic circuits", Optics Express Vol. 22, Issue 17, pp. 20652-20662 (2014) doi: 10.1364/OE.22.020652
[10] www.plcconnections.com, PLC Connections, Columbus OH, USA.
[11] http://mapleleafphotonics.com, Maple Leaf Photonics, Seattle WA, USA.